Large-Scale Synthesis of TiO2 Microspheres with Hierarchical Nanostructure for Highly Efficient Photodriven Reduction of CO2 to CH4

ARTICLE *in* ACS APPLIED MATERIALS & INTERFACES · AUGUST 2014

Impact Factor: 6.72 · DOI: 10.1021/am504128t · Source: PubMed

6 AUTHORS, INCLUDING:

Baizeng Fang
University of British Columbia - Vancouver
101 PUBLICATIONS **2,236** CITATIONS
SEE PROFILE

Arman Bonakdarpour
University of British Columbia - Vancouver
50 PUBLICATIONS **1,577** CITATIONS
SEE PROFILE

Kevin Reilly
University of British Columbia - Vancouver
2 PUBLICATIONS **10** CITATIONS
SEE PROFILE

Yalan Xing
Beihang University(BUAA)
28 PUBLICATIONS **201** CITATIONS
SEE PROFILE

ACS APPLIED MATERIALS & INTERFACES

Research Article

www.acsami.org

Large-Scale Synthesis of TiO_2 Microspheres with Hierarchical Nanostructure for Highly Efficient Photodriven Reduction of CO_2 to CH_4

Baizeng Fang,[†,‡] Arman Bonakdarpour,[†,‡] Kevin Reilly,[†,‡] Yalan Xing,[†,‡] Fariborz Taghipour,[†,‡] and David P. Wilkinson*[,†,‡]

[†]Department of Chemical & Biological Engineering, University of British Columbia, 2360 East Mall, Vancouver, British Columbia, Canada V6T 1Z3

[‡]Clean Energy Research Center, 2360 East Mall, Vancouver, British Columbia, Canada V6T 1Z3

Supporting Information

ABSTRACT: In this study, a simple and reproducible synthesis strategy was employed to fabricate TiO_2 microspheres with hierarchical nanostructure. The microspheres are macroscopic in the bulk particle size (several hundreds to more than 1000 μm), but they are actually composed of P25 nanoparticles as the building units. Although it is simple in the assembly of P25 nanoparticles, the structure of the as-prepared TiO_2 microspheres becomes unique because a hierarchical porosity composed of macropores, larger mesopores (ca. 12.4 nm), and smaller mesopores (ca. 2.3 nm) has been developed. The interconnected macropores and larger mesopores can be utilized as fast paths for mass transport. In addition, this hierarchical nanostructure may also contribute to some extent to the enhanced photocatalytic activity due to increased multilight reflection/scattering. Compared with the state-of-the-art photocatalyst, commercial Degussa P25 TiO_2, the as-prepared TiO_2 microsphere catalyst has demonstrated significant enhancement in photodriven conversion of CO_2 into the end product CH_4. Further enhancement in photodriven conversion of CO_2 into CH_4 can be easily achieved by the incorporation of metals such as Pt. The preliminary experiments with Pt loading reveal that there is still much potential for considerable improvement in TiO_2 microsphere based photocatalysts. Most interestingly and significantly, the synthesis strategy is simple and large quantity of TiO_2 microspheres (i.e., several hundred grams) can be easily prepared at one time in the lab, which makes large-scale industrial synthesis of TiO_2 microspheres feasible and less expensive.

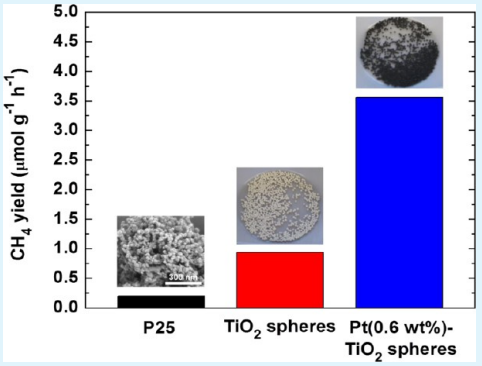

KEYWORDS: *TiO_2 spheres, hierarchical nanostructure, Pt loading, photocatalyst, CO_2 reduction*

1. INTRODUCTION

Although carbon dioxide is the least potent of all the greenhouse gas (GHG) emissions, it is the most important in terms of its contribution to climate change. The rapid increase in the level of anthropogenic CO_2 resulting in global climate change is a matter of great concern. Turning CO_2 into a clean energy fuel would be a solution for both the shortage of fossil fuels and the global warming problem. Hence, this is an energy research topic of great interest. However, the process for turning CO_2 into fuels is energy intensive and useful only if a renewable energy source can be used for the purpose. Therefore, a potential avenue for sustainable development is to use photocatalysts for the conversion of CO_2 into hydrocarbon fuels with the help of solar energy, a clean and renewable energy source.

Titania has been considered a particularly appropriate candidate for photocatalytic processes due to its powerful oxidation properties, superior charge transport properties, and corrosion resistance.[1−12] Furthermore, it is readily available and less expensive compared with other photocatalyst candidates such as gallium−phosphide semiconductors[13,14] and transition metal complexes, such as ruthenium(II) polypyridine carbonyl complex,[15] cobalt(II) trisbipyridine,[16] and rhenium(I) bipyridine (bpy) complexes, fac-[Re(bpy)$(CO)_3$L] (L = SCN- (1-NCS), Cl- (1-Cl), and CN- (1-CN)).[17] Due to its attractive properties such as nontoxicity, high availability, low cost, and long-term stability against photo and chemical corrosion, titania has attracted much attention in recent years as a photocatalyst in "artificial photosynthesis", i.e., photoassisted water splitting[18,19] and CO_2 conversion.[20] Other applications include the degradation of organic pollutants,[8] water disinfection and purification, hazardous waste remediation, and air purification.[21,22] Various TiO_2-based materials have been investigated for photoassisted CO_2 conversion, but to date, mainly commercial Degussa P25[23−25] and TiO_2 nanotubes (NTs)[26,27] have been used. However, these TiO_2-based

Received: June 26, 2014
Accepted: August 20, 2014
Published: August 20, 2014

materials are either time-consuming and costly to produce[26,27] and/or cannot efficiently drive the CO_2 conversion reaction without an appropriate co-catalyst due to the wide energy gap of TiO_2.[23−25] Incorporating transition metals is an effective method to tailor and engineer the structure, phase, and band gap. Copper is considered as one of the most suitable options since both cupric oxide and cuprous oxide are p-type semiconductors with a narrower band gap.[28] Additional promising metals for dopants are Fe[29] and Sn.[30]

In addition to the problem caused by the wide energy gap of TiO_2, low photocatalytic activity for TiO_2-based materials can result from the recombination of the electron−hole pairs generated by photo irradiation. Generally, the electron−hole pairs generated by solar irradiation and their lifetime are key factors for the photocatalytic reaction and efficiency. Titania has so far yielded only low carbon dioxide conversion rates despite using ultraviolet illumination for band gap excitation,[26] which is not practical for the commercialization of CO_2 reduction. Therefore, considerable enhancement in photocatalytic activity of TiO_2-based photocatalyts is required. An efficient approach to reduce the recombination rate of the electron−hole pairs is to disperse TiO_2 onto a substrate (i.e., support) such as carbon NTs, which function as dispersing agents to prevent the TiO_2 nanoparticles (NPs) from agglomerating and hence decrease the recombination rate of the electron−hole pairs.[31] Other strategies include doping noble metals such as Ru,[32] Pd,[33,34] or Pt[26] onto TiO_2, which can change the distribution of electrons and effectively prevent the electron−hole recombination.

Current photocatalysts for CO_2 reduction are inefficient. State-of-the-art CO_2 photoreduction catalysts do not perform as efficiently as the state-of-the-art catalysts for H_2 photogeneration.[35] Therefore, it is highly desirable to develop novel photocatalysts with high catalytic activity toward CO_2 photoreduction. Recently, Wang et al. reported photoreduction of CO_2 using CdSe/Pt/TiO_2 heterostructured catalysts.[36] Although costly catalysts were utilized and complicated synthesis procedures involved, due to the irradiation under visible light, photoreduction efficiency of CO_2 was still low compared with that obtained under UV irradiation. More recently, Liu et al. reviewed engineering TiO_2 nanomaterials for CO_2 conversion,[37] and Mori et al. commented on photocatalytic reduction of CO_2 with H_2O on various titanium oxide photocatalysts.[38]

In this study, novel TiO_2-based spherical photocatalysts with large mesoporous volume and hierarchical porosity are designed and developed to improve the photocatalytic activity and efficiency for solar reduction of CO_2. The synthesis strategies for the TiO_2 spheres and Pt-loaded ones are relatively simple, scalable and reproducible. Interestingly, compared with the widely used benchmark photocatalyst, commercial Degussa P25 TiO_2, the TiO_2 microsphere photocatalyst demonstrates remarkably enhanced photocatalytic activity toward photodriven CO_2 reduction to CH_4 due to its large surface area and particularly the unique hierarchical porosity, facilitating fast mass transport. In addition, the hierarchical nanostructure may also contribute to the improved photocatalytic activity due to enhanced multilight reflection/scattering. Furthermore, further improvement in photodriven conversion of CO_2 can be realized readily through a simple approach, incorporation of metals such as Pt.

Compared with nanosized TiO_2 catalysts reported by other researchers, the TiO_2 microspheres with larger particle size (several hundreds to more than 1000 μm) developed in this study are self-supported (i.e., they do not need a supporting substrate). The TiO_2 microspheres possess advantages over other nanoscaled materials, such as commercial P25 NPs. The TiO_2 microspheres with macroscopic particle size do not have a particle agglomeration issue, making handling much simpler (i.e., no need to make pellets or to make a thin film on a substrate). From the viewpoint of some practical applications, the TiO_2 microspheres catalyst is a very good functional material design, making large-scale synthesis and application of photocatalyst feasible. Furthermore, this photocatalyst possesses excellent mechanical strength,[39] and thus is better suited for a fluidization bed reactor which is an inherently scalable and favorable reactor for industrial use.

2. EXPERIMENTAL SECTION

2.1. Synthesis of Photocatalysts. TiO_2 spheres with large particle size (greater than 500 μm) were synthesized through a modified TiO_2 sol−gel approach[18,39] as illustrated in Figure 1.

Figure 1. Illustration for the synthesis of TiO_2 spheres.

Typically, 96 mL of C_2H_5OH was mixed with 6.4 mL of deionized H_2O (DI), followed by the addition of 16 mL of concentrated HCl (Fisher, 37%) and 120 mL of titanium isopropoxide (TTIP) (Sigma-Aldrich, 97%) while the solution was vigorously stirred. After the solution stirred for 2 h at 360 rpm, 38 g of precalcined Degussa P25 powder was then introduced to the sol−gel solution and the resulting P25 in Ti(IV) sol−gel was stirred overnight. Next, a chitosan glacial acetic acid aqueous solution (1 wt %) was introduced to the sol−gel in the volume ratio of 2:1. After it stirred for 2 h, the resulting mixture was then added dropwise from a modified buret into a basic NH_4OH (Fisher, 30%) aqueous solution (6 vol %). TiO_2 spheres were produced and collected from the basic solution and calcined at 450 °C for 3 h. In the synthesis, commercial P25 TiO_2 was dispersed in the sol as filler to fabricate composite high performance sol−gel materials. P25 TiO_2 was chosen because of its high photoefficiency to degrade organic pollutants.

Pt-loaded TiO_2 spheres with various Pt contents were prepared through a microwave-assisted synthesis strategy using ethylene glycol (EG) as the reducing agent.[40−42] The Pt-loaded catalysts were thoroughly washed with ethanol and DI water to remove any residual EG.

2.2. Physical Characterization. N_2 adsorption and desorption isotherms were measured at 77 K on a Micromeritics ASAP-2020 Gas Adsorption Analyzer after a sample was degassed at 423 K to 20 mTorr for 12 h. The specific surface areas were determined from nitrogen adsorption using the Brunauer−Emmett−Teller (BET) method. Total pore volumes (V_{Total}) were determined from the amount of gas adsorbed at a relative pressure of 0.99. Micropore volume (V_{Micro}) and micropore size of the porous materials were calculated from the analysis of the adsorption isotherms using the Horvath−Kawazoe (HK) method. Pore size distribution (PSD) was

calculated from the adsorption branches by the Barrett–Joyner–Halenda (BJH) method.

Surface morphologies of the various TiO_2-based catalysts were examined by a scanning electron microscope (SEM) FEI Helios NanoLab 650 FIB-SEM or by a Cameca SX-50 Scanning Electron Microprobe with 4 vertical wavelength-dispersion X-ray spectrometers and a fully integrated SAMx energy-dispersion X-ray spectrometer.

X-ray diffraction (XRD) patterns were obtained on a Siemens D5000 (Vantec detector) and Bruker D8 Focus (LynxEye detector) X-ray powder diffractometers by using Co Kα radiation as the X-ray source, operating at 35 kV and 40 mA. The diffractograms were recorded in the 2θ range 10–80°, in steps of 0.02° with a count time of 20 s at each point. The particle size was determined from the broadening of the diffraction peak using the Scherrer formula, $D = K\lambda/\beta \cos\theta$, where D is the crystallite size (nm), K is the Scherrer constant, λ is the wavelength of the X-ray source, β is the full width at half-maximum, and θ is the Bragg angle.

X-ray photoelectron spectroscopy (XPS) measurements were made with a Leybold MAX200 spectrometer using a Mg Kα source (1253.6 eV) operated at 15 kV and 20 mA. All binding energies were corrected for sample charging by referencing to the adventitious C 1s peak at 285.0 eV.

A Varian Cary 4000 UV–visible diffuse reflectance spectrophotometer was employed to obtain UV–visible diffuse reflectance spectra (UV–vis DRS) for various photocatalysts over a spectral range of 200–800 nm.

2.3. Photodriven Reduction of CO_2. The use of titania and water (without sacrificial hole scavengers) ultimately provides a green chemistry approach for the photoconversion of CO_2 to fuels.[43,44] In this study, water was used as the only electron donor.

A batch reactor of 39 mm in diameter and 9 mm in depth was made for photocatalytic conversion of CO_2 with water. For a typical run, a mixture of 200 mg of catalyst mixed with 100 μL of H_2O was placed in a container (20 mm in diameter) located in the center of the reactor. After the introduction of pressurized CO_2 (50 PSI) (or N_2, for blank experiments only; will be explained later in this section), the reactor was irradiated with a Hg UV lamp (40 W, 254 nm, light intensity at the location of catalyst: 20 mW cm^{-2}) for a 24 h period. The gas products were collected through a 10 mL syringe and injected into a gas chromatograph (SRI 8610 Gas Chromatograph, Mandel, Canada), which was equipped with FID and TCD detectors for the detection of CH_4, CO, and H_2, respectively. Because this study focused on CO_2 photoreduction on a gas–solid interface, possible liquid products like methanol, formaldyhyde and formic acid, which are more likely generated in aqueous solutions, were not measured. For each type of catalyst, experiments were carried out at least three times using fresh catalyst each time. The production rates are averaged and reported with standard deviations.

Stability tests were conducted for the used photocatalysts after being removed from the reactor followed by storage in air at room condition for 24 h. Then, the used photocatalysts were placed back in the reactor without further treatment.

Prior to any photocatalytic conversion of CO_2 with water, all the reported catalysts in this study had been examined in blank experiments to make sure that there was no carbon-containing product produced without introduction of CO_2 into the reactor. The results from the blank experiments confirm that the carbon-containing gas products (i.e., CO, CH_4, etc.) were produced from the photoreduction of CO_2 only, not from residual carbon-containing organics in the catalysts.

The digital photographs for the experimental setup are shown in Figure S1 (Supporting Information).

3. RESULTS AND DISCUSSION

Figure 2 shows digital photograph and representative SEM images for the as-prepared TiO_2 spheres. As shown in Figure 2A, the TiO_2 spheres take on a yellowish color. The SEM image in Figure 2B reveals that the TiO_2 spheres have a diameter of ca. 1.3 mm, and generally, the outer surface of the sphere is

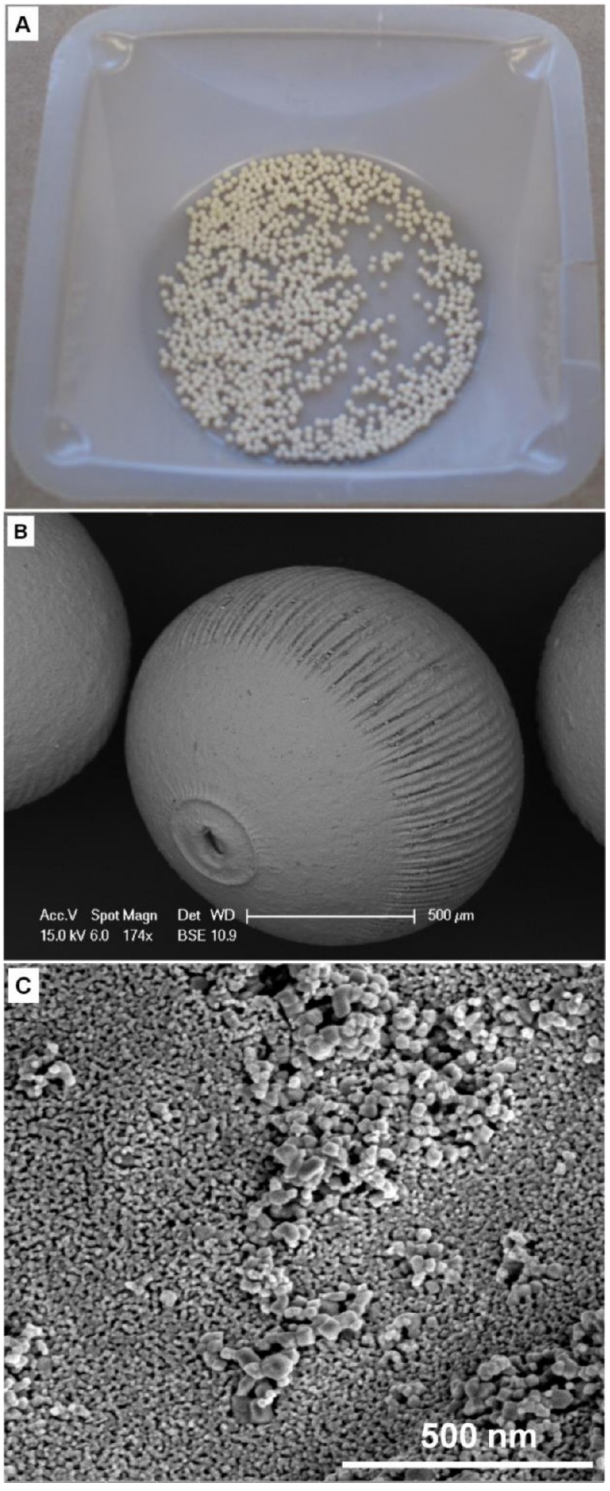

Figure 2. Digital photograph (A), and SEM images with various magnifications (B and C) for the as-prepared TiO_2 spheres.

smooth. The magnified image (Figure 2C) shows that the most of the outer surface is densely packed with small particles of ca. 12–28 nm. In some areas, larger particles of ca. 58–86 nm were also observed. In addition, mesopores (voids) in the range from ca. 10 to 50 nm are clearly observed, which are formed by the aggregated particles. Interestingly, it was also found that through controlling the rate for the addition of the mixture of P25 in Ti(IV) sol–gel into the ammonia solution, the particle size of the obtained TiO_2 spheres could be effectively

controlled, as shown in Figure S2 (Supporting Information). In contrast, the commercial Degussa P25 shows the agglomeration of TiO_2 NPs of ca. 15−50 nm, as evident in Figure S3 (Supporting Information).

Representative nitrogen adsorption−desorption isotherms for the as-prepared TiO_2 spheres (ca. 1.3 mm in diameter) are shown in Figure 3A. They can be classified as a type IV

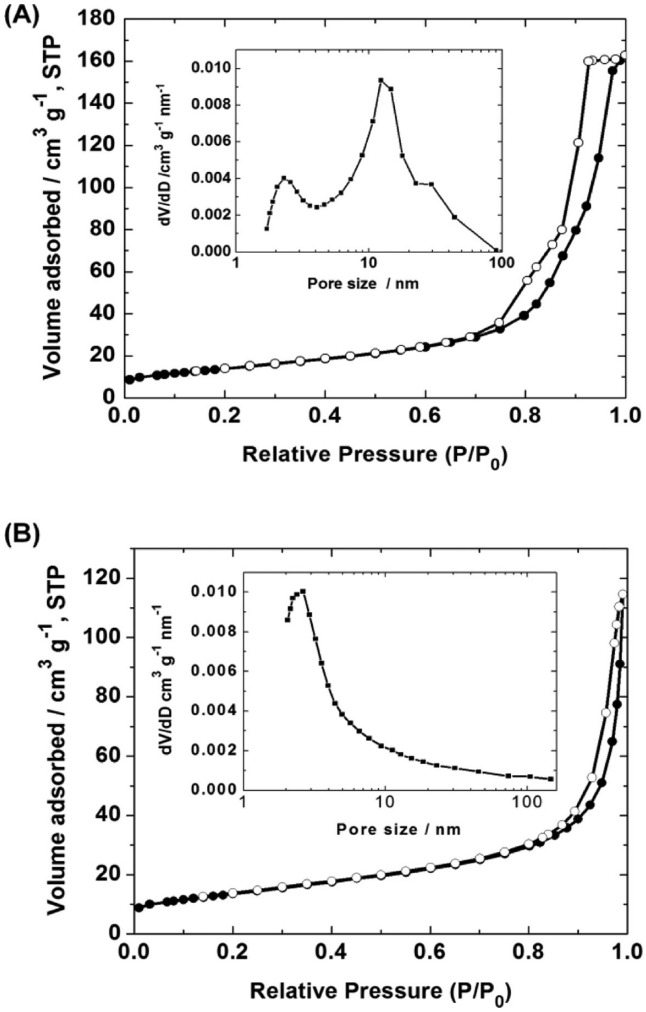

Figure 3. Representative nitrogen adsorption−desorption isotherms at 77 K and derived PSD for the as-prepared TiO_2 spheres (A) and commercial P25 TiO_2 (B).

isotherm with a type H2 hysteresis loop, according to the BDDT (Brunauer, Deming, Deming and Teller) classification. The TiO_2 spheres sample reveals a BET surface area of ca. 50.2 $m^2\ g^{-1}$, a mesoporous volume of ca. 0.253 $cm^3\ g^{-1}$ and a negligible micorporous volume. Interestingly, the sample demonstrates a hierarchical porosity composed of macropores (greater than 50 nm), larger mesopores with a PSD maximum located at ca. 12.4 nm, and smaller mesopores of ca. 2.3 nm. The pore size measured by the BET measurement is in good agreement with that observed from the SEM image shown in Figure 2C. As shown in Figure 3B, the P25 TiO_2 sample shows a type H3 hysteresis, indicating the presence of mesopores. The PSD reveals that P25 has a single size distribution with a PSD maximum located at ca. 2.6 nm, which is much smaller that the larger mesopores (ca. 12.4 nm) observed for the TiO_2 spheres. The P25 TiO_2 has a BET surface area of ca. 48.4 $m^2\ g^{-1}$, which is slightly smaller than that of the as-prepared TiO_2 spheres. In addition, the P25 sample has a mesoporous volume of ca. 0.180 $cm^3\ g^{-1}$, which is significantly smaller than that (i.e., 0.253 $cm^3\ g^{-1}$) measured for the TiO_2 spheres, and also a negligible microporous volume. The larger surface area and mesoporous volume, and particularly the hierarchical porosity, would be expected to improve the photocatalytic activity of the TiO_2 spheres catalyst.

To further enhance photocatalytic conversion efficiency, the as-prepared TiO_2 spheres were decorated with Pt. SEM images for some representative Pt-incorporated TiO_2 sphere catalysts are shown in Figure 4. It is evident that with increasing Pt content there is more coverage of the outer surface of the TiO_2 spheres with Pt particles, which grow in size and result in some agglomeration. When the Pt content is as low as 0.3 wt %, the Pt NPs size is ca. 5−10 nm (Figure 4A), while the size increases to 8−16 nm (Figure 4B) when the Pt content reaches 0.6 wt %. Although the size increases, Pt NPs still disperse uniformly on the substrate. However, when the Pt content is further increased to 0.9 wt %, the size of the Pt NPs increases significantly and reaches 18−22 nm (Figure 4C) with some agglomeration. When the Pt content increases to 1.8 wt %, Pt NPs are found to have a mean size of ca. 24 nm as shown in Figure 4D and Figure S4 (Supporting Information), which is ca. twice that observed for the Pt (0.6 wt %)/TiO_2. Interestingly, compared with Pt (1.8 wt %)/TiO_2, the Pt NPs in Pt (0.6 wt %)/TiO_2 have a much smaller particle size (average ca. 12 nm) and a more uniform dispersion on the TiO_2 surface, as shown in Figure 4B.

XRD data shown in Figure 5A reveals the TiO_2 spheres catalyst has a similar pattern to that of the commercial P25 sample except that the former reveals stronger diffraction peaks for the anatase phase, suggesting larger crystalline size. The data also reveal that the TiO_2 spheres catalyst consists of 79% anatase TiO_2 with a crystalline size of 19 nm and 21% rutile TiO_2 with a crystalline size of 75 nm. Thus, the dominant phase in the TiO_2 spheres is anatase, similar to P25. XRD patterns for the Pt-incorporated TiO_2 spheres with various Pt contents are shown in Figure 5B. For a clear comparison and better understanding, Pt black was also characterized by XRD measurement, and the data is shown in Figure S5 (Supporting Information). It was found that in the scanned range, Pt has a reflection peak Pt(111) located at 46.6° and a reflection peak Pt(200) located at 54.4 °. However, from Figure 5, only anatase and rutile TiO_2 phases were observed for the Pt-loaded TiO_2 samples, and no separate Pt-related reflection peak was shown even for the Pt (1.8 wt %)/TiO_2. This phenomenon has been reported for Pt-incorporated TiO_2 materials when Pt contents are lower than 4 wt %.[45,46] This can be explained because Pt(IV) has an ionic radii of 0.625 Å, which is comparable to that of Ti(IV) (0.605 Å). Thus, it is energetically favorable for Pt ions to occupy Ti(IV) sites.[47] In addition, the Pt loadings may be too low to be detected by laboratory-based XRD with a typical detection limit of 5 wt %.

XPS data shown in Figure 6A reveal that P25 TiO_2 and the TiO_2 spheres are composed of pure TiO_2. For the Pt-loaded sample, the peaks for Pt 4d and 4f are clearly observed even for the sample with low Pt content (i.e., 0.3 wt %). The doublet peaks shown in the magnified Pt 4f spectrum (Figure 6B) were observed at 71.2 and 74.6 eV, which are attributable to 4f7/2 and 4f5/2 of metallic Pt, respectively, implying that the dominant valences of the Pt species in the catalysts are zero. After the deconvolution of the magnified XPS spectrum for Pt

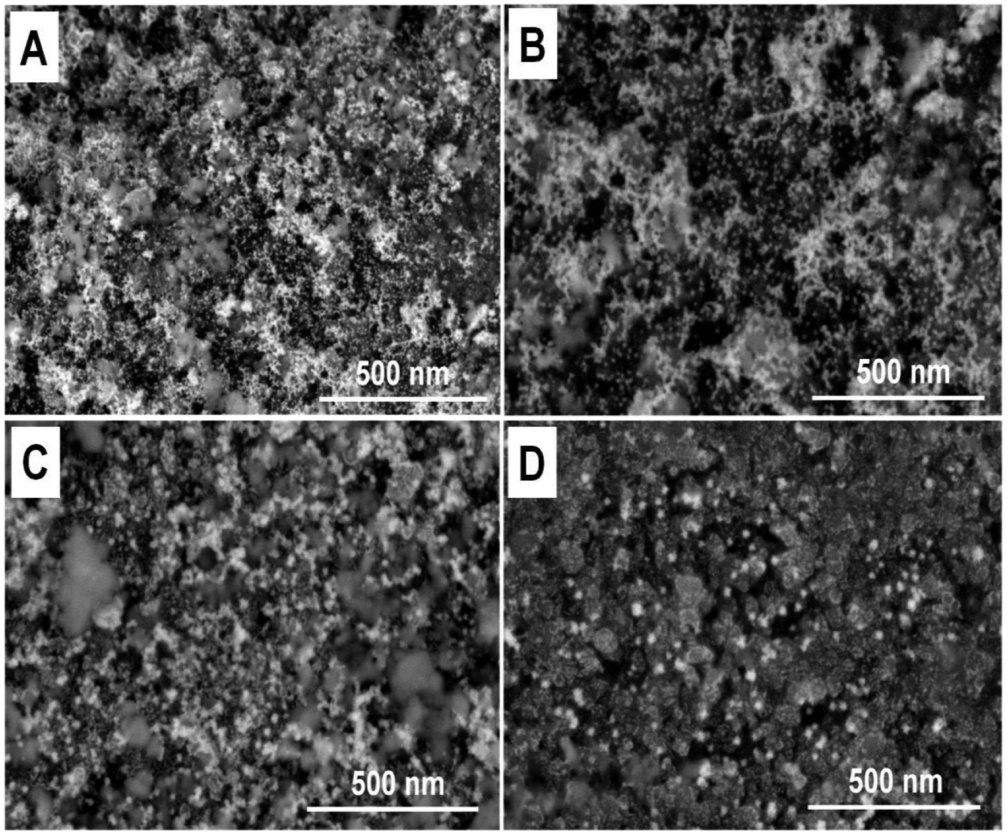

Figure 4. SEM images for the Pt−TiO_2 spheres catalysts with various metal loadings: (A) 0.3, (B) 0.6, (C) 0.9, and (D) 1.8 wt %.

4f, it was also found that the deposited Pt NPs on the outer surface of the Pt (0.3 wt %)/TiO_2 are composed of 76% of Pt (0), 16% of Pt (II) and 8% of Pt(IV).

Various TiO_2-based catalysts were investigated for photodriven CO_2 reduction with water. Table 1 summarizes yields of the gas products for the P25 and spherical TiO_2 photocatalysts without Pt loading.

The P25 catalyst shows a production yield of 0.20, 2.31, and 1.72 μmol g(catalyst)$^{-1}$ h^{-1} for CH_4, CO, and H_2, respectively, while the as-prepared TiO_2 spheres catalyst produces 0.94, 2.32, and 2.03 μmol g^{-1} h^{-1} of CH_4, CO, and H_2, respectively. Intermediate product CO is identified as the major carbon-containing gas product for the photodriven reduction of CO_2 with H_2O for the plain TiO_2 catalysts, which has also been observed by other researchers.[48,49] In addition, it was also found that when P25 and the plain TiO_2 spheres were used as a photocatalyst, no C_2H_6, ethylene, or acetylene was detected. The phenomenon observed for the commercial P25 is consistent with that reported by Tan et al.[24] It is well-known that CH_4 is the end product for the photocatalytic reduction of CO_2, and thus, it has more significance than the intermediate products like CO. The as-prepared TiO_2 microsphere catalyst and commercial P25 catalysts are very close in specific surface area, as revealed by the BET measurements. Therefore, the enhanced selectivity of CH_4 production observed for the as-prepared TiO_2 microsphere catalyst is mainly attributable to the larger mesoporous volume and particularly the hierarchical pore structure composed of macropores, larger mesopores (ca. 12.4 nm) and smaller mesopores (ca. 2.3 nm). Compared with the commercial P25 NPs catalyst, the as-prepared TiO_2 microsphere catalyst is advantageous and superior because numerous meospores with large pore size have been developed throughout the whole microsphere during the assembly of P25 NPs. These large mesopores can be considered as hollow channels, facilitating fast mass transport within the TiO_2 microsphere. Zhao et al. reported that the multichannel hollow structure in TiO_2 fibers induces not only an inner trap effect on gaseous molecules, but also a multiple-reflection effect on incident light, which further improves the photocatalytic activity of TiO2 hollow fibers.[50] Therefore, the hierarchical nanostructure developed in the TiO_2 microsphere not only favors fast mass transport, resulting in enhanced photocatalytic activity, but may also contribute to the improved photocatalytic activity due to the enhanced multilight scattering. This creates a greater possibility for multielectron reaction, i.e., eight electrons for CH_4 generation. Thus, the as-prepared TiO_2 microsphere is completely different from other TiO_2 bulk materials without highly developed mesopores, in which only a few micrometers of the TiO_2 outer surface can be utilized for light harvesting, resulting in low photodriven CO_2 conversion into CH_4. Clearly, the TiO_2 microspheres have particularly unique features: they not only maintain the nanoscale properties from the building units of P25 TiO_2 NPs, but also benefit from additional collective properties at the macroscopic scale, namely, the hierarchical porosity developed during the assembly of TiO_2 NPs. Other researchers have also suggested that hierarchical nanostructures for photocatalysts improve photocatalytic activity. Zhu et al. reported that the hierarchical structures of photocatalysts contribute significantly to the absorption enhancement under visible light.[51,52] Wang et al. also reported that nanoporous SnO_2 catalyst containing two types of porous structures has higher photocatalytic activity than Degussa P25 for degrading methyl orange.[9] Li et al. reported that the

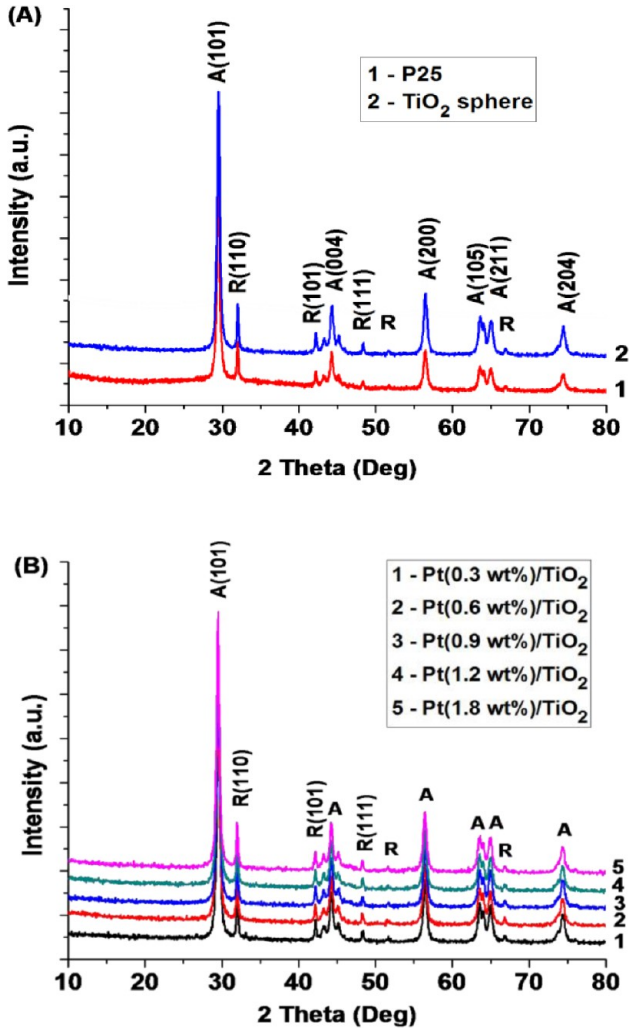

Figure 5. XRD patterns for plain TiO_2 samples (A), and for Pt incorporated TiO_2 spheres with various metal contents (B).

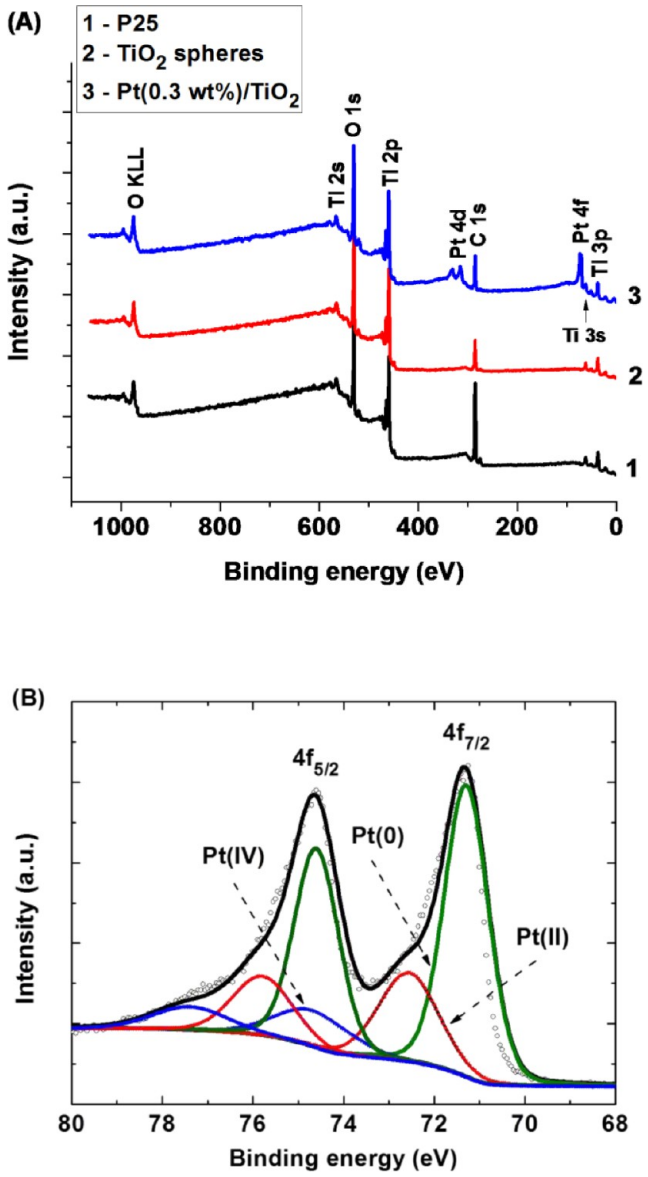

Figure 6. XPS spectra for the various TiO_2 based catalysts (A), and the deconvolution of Pt 4f doublet for Pt (0.3 wt %)/TiO_2 spheres (B).

multilight scattering demonstrated by hierarchical nanostructured TiO_2 contributes to enhanced photocatalytic activity.[53,54]

After the exposure to ambient air in the room environment for 24 h, the used photocatalysts show slightly decreased production yields for all the gas products, resulting from the accumulation of carbonaceous compounds. A similar phenomenon has also been observed by other researchers for TiO_2-based photocatalysts employed for photodriven CO_2 reduction with H_2O.[48] However, the results from the stability tests indicate that the used catalysts have been largely regenerated during ambient air exposure due to desorption of the gas products from the surface of the catalysts.

Pt has been frequently used as a photocatalytic promoter, which can effectively change the distribution of electrons and reduce the electron−hole recombination reaction.[26] Figure 7 shows the data obtained for the spherical TiO_2 catalysts with various Pt loadings.

Compared with the P25 catalyst, the plain TiO_2 spheres catalyst shows greatly enhanced photocatalytic activity toward the reduction of CO_2, i.e., about 5 times as much CH_4 is produced by the plain TiO_2 spheres catalyst. After Pt loading, the TiO_2 spheres catalyst produces an even higher concentration of H_2 because Pt prevents the recombination of electron−hole pairs, which in turn increases the photocatalytic

Table 1. Yield (μmol g(catalyst)$^{-1}$ h^{-1}) of the Gas Products (H_2, CO, and CH_4) Produced during 24 h of Photodriven CO_2 Reduction on the Various Pure TiO_2 Catalysts[a]

gas	P25		TiO_2 spheres	
product	fresh	used[b]	fresh	used[b]
CH_4	0.20	0.18	0.94	0.87
CO	2.31	1.98	2.32	2.06
H_2	1.72	1.56	2.03	1.95

[a]Experimental conditions: 200 mg of catalyst mixed with 100 μL of DI water, pressurized CO_2 (50 PSI), UV (20 mW/cm^2, 254 nm). [b]A used catalyst means it has been run for one test.

production of H_2. It was reported that H_2 can work as another reductant to facilitate the reduction of CO_2 to CH_4. Lo et al. reported that hydrogen molecules can be adsorbed dissociatively to form H^+ on the surface of TiO_2 and supplied as a hydrogen atom to convert CO_2 to hydrocarbons by photoreduction.[23] H^+ would further react with an e^- to produce $^{\bullet}H$

dx.doi.org/10.1021/am504128t | ACS Appl. Mater. Interfaces 2014, 6, 15488−15498

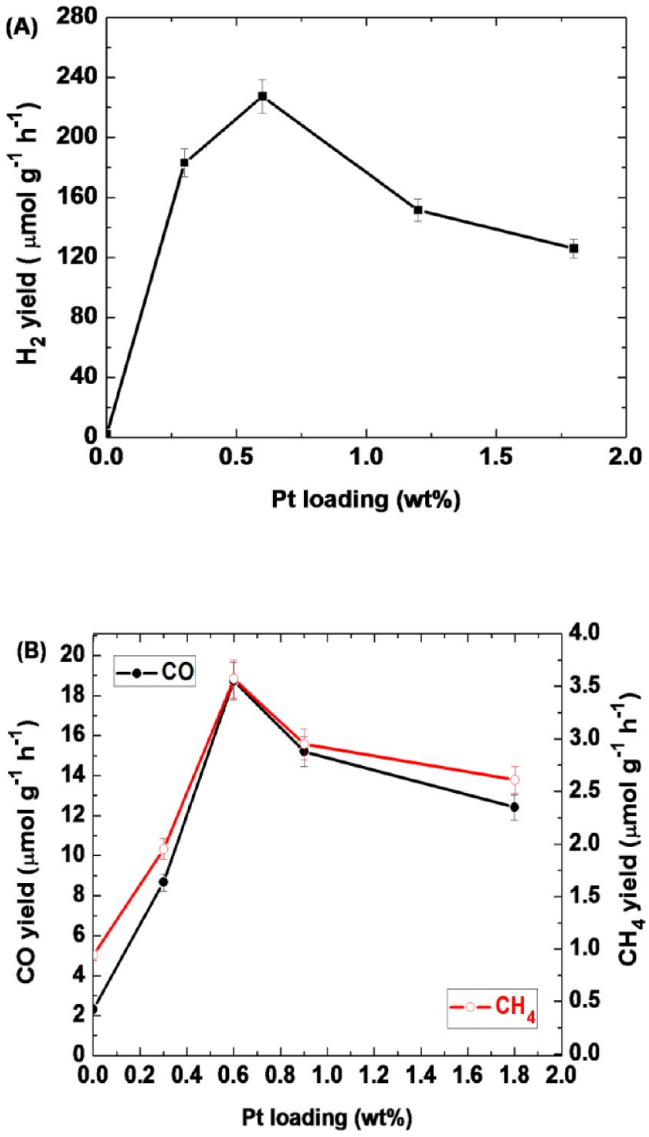

Figure 7. Yields of the gas products (H_2, CO and CH_4) produced during 24 h of photodriven CO_2 reduction on TiO_2 sphere catalysts with various Pt loadings. Experimental conditions: 200 mg of catalyst mixed with 100 μL of DI water, pressurized CO_2 (50 PSI), UV (20 mW/cm^2, 254 nm).

radicals. The •H radicals are a highly reactive species, which directly react with CO_2 and accelerate its reduction. Therefore, it is clear that with the increasing H_2 content, the CH_4 produced is expected to increase. Due to the much larger amount of H_2 produced by the Pt-loaded TiO_2 catalysts, more CH_4 is produced. As seen from Figure 7, the amount of CH_4 and CO produced by the Pt-loaded TiO_2 catalysts is higher than that produced by the plain TiO_2 catalysts (i.e., P25 and TiO_2 spheres), which indicates that Pt-loaded TiO_2 catalysts have much higher catalytic activity toward the solar reduction of CO_2 than the plain ones.

In addition, other hydrocarbons such as C_2H_6 and/or C_2H_4 have also been reported to be produced through other reaction paths[23] when the H_2 concentration is high in the reaction system. This explains why C_2H_6 and C_2H_4 were produced by the Pt-loaded TiO_2 catalysts. It is also interesting to note that the H_2 and CH_4 amounts produced by the Pt-loaded TiO_2 catalysts increase with increasing Pt content up to 0.6 wt %, and then decreased with a further increase in the Pt content. While the addition of platinum allows the hydrogen evolving reaction to proceed, platinum deposits also catalyze the back reaction of hydrogen and oxygen to form water and heat, which becomes dominant at some level of Pt loading, thus reducing the overall efficiency of the system.[18,51] In addition, with an increase in the Pt loading, Pt NPs increase in size, resulting in worse particle dispersion on the TiO_2 spheres substrate, which not only lowers the catalytic efficiency of Pt, but also results in lower light harvesting due to the shadowing of the photocatalyst particle (TiO_2) by surface platinum deposits. This is evident from the comparison of the SEM images shown in Figure 4B for Pt (0.6 wt %)/TiO_2 and Figure S4 for Pt (1.8 wt %)/TiO_2. From Figure S4 it was found that most of the surface of the TiO_2 particles is covered by the Pt NPs.

According to the reactions 1 and 2 given below, 2 and 8 mol of electrons are consumed for the production of 1 mol of CO and CH_4, respectively.

$$CO_2 + 2H^+ + 2e^- \rightarrow CO + H_2O \quad (1)$$

$$CO_2 + 8e^- + 8H^+ \rightarrow CH_4 + 2H_2O \quad (2)$$

The apparent quantum yield (Φ) for the gas products CO and CH_4 can be calculated according to the following equation:[48]

$$\Phi_{product}(\%) = (n \text{ mol of product yield/moles of photons absorbed by catalyst}) \times 100\%$$

here, n = 2 for CO and 8 for CH_4.

For the fresh P25 TiO_2 catalyst, Φ based on the average production yield was calculated to be 0.204% and 0.072% for CO and CH_4, respectively. For the fresh plain TiO_2 spheres catalyst, Φ was calculated to be 0.204% and 0.340% for CO and CH_4, respectively. When Pt (i.e., 0.6 wt %) is incorporated, Φ significantly increases up to 1.632% and 1.315% for CO and CH_4, respectively.

On the basis of the production rate of the end product CH_4 produced, it is interesting to note that the TiO_2 spheres catalyst exhibits 4 to 5 times the conversion rate for CO_2 reduction that can be obtained by the commercial Degussa P25 TiO_2. Higher photocatalytic activity observed for the plain spherical TiO_2 catalyst may be mainly attributed to larger surface area, larger mesoporoous volume, and particularly the hierarchical multimodal pore structure. Usually, for a TiO_2-based photocatalyst, a larger surface area can offer more active adsorption sites and photocatalytic reaction centers. Larger mesoporous volume and the hierarchical pore structure composed of macropores, larger mesopores (ca. 12.4 nm), and smaller mesopores (ca. 2.3 nm) enhance the adsorption efficiency of light and the diffusion of the gas molecules. This behavior has been frequently observed by other researchers. Wang et al. proposed a multiple reflection mechanism and fast mass transport for hierarchically structured photocatalysts.[55] They claimed that the macrochannels in the hierarchically structured photocatalysts may exhibit two beneficial effects on titania, namely, increasing the efficiency of photoabsorption and improving mass transfer. In the macro/mesoporous TiO_2 photocatalyst, the macrochannels could act as a light-transfer path to introduce incident photon flux onto the inner surface of mesoporous TiO_2, and enable light to penetrate deep inside the photocatalyst, thus making it a more efficient light harvester. Considering the light absorption, reflection, and scattering within such a hierarchical porous

system, the effective light-activated surface area could be significantly enhanced. The enhanced multiple-light reflection mechanism in hierarchical nanostructured materials was experimentally supported in Wang's paper by the UV−vis DRS of the titanium dioxide materials with/without a hierarchical nanostructure. They also claimed that the transport of small molecules in media featuring large mesopores (>10 nm) and macropores can approach rates of diffusion comparable to those in an open medium, and thus assumed that the macrochannels in their samples can act as effective transport paths for reactants. Such transport enhancement is very important for the application of mesoporous titania in gas-phase photocatalysis. In another example, Liu et al. synthesized nanoplates-assembled hierarchical Bi_2WO_6 flowers for photocatalysis application.[56] They claimed that the specific hierarchical configuration, along with the bimodal mesoporous microstructure of the multilayered flower-like assemblies allows multiple scattering of UV−visible light within their frameworks, giving them even greater light-harvesting capacities. The optical path length for light transporting through the Bi_2WO_6 hierarchical multilayered flowerlike assemblies may be longer than that for nanoplates due to multiple scattering, resulting in a greater absorbance.

From the literature[50,56,57] it is very evident that hierarchical nanostructured materials composed of macropores in combination with large mesopores (>10 nm) can favor improved photoabsorption due to enhanced multiple light refection/scattering.

Interestingly, in our study it is also evident that the hierarchical nanostructured TiO_2 (i.e., the as-synthesized TiO_2 microspheres) demonstrate enhanced photoabsorption compared with TiO_2 without a hierarchical nanostructure (i.e., P25 TiO_2), as shown in Figure 8. This can be attributed to the hierarchical nanostructure composed of macropores (>50 nm) and large mesopores (ca. 12.4 nm) in the as-synthesized TiO_2 microsphere catalyst.

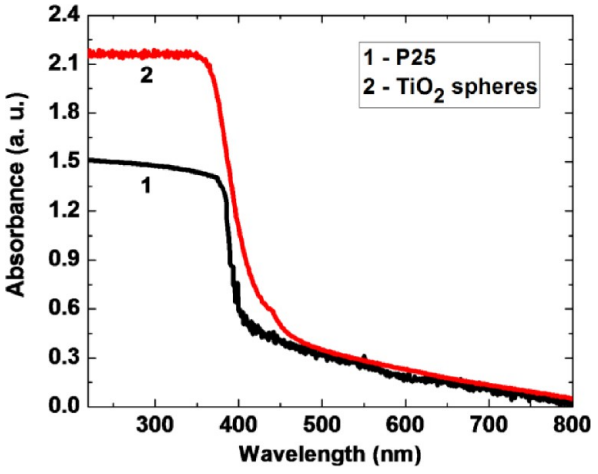

Figure 8. UV−vis diffuse reflectance spectra for P25 TiO_2 and the as-synthesized TiO_2 microsphere.

In addition, surface defect sites generated during the synthesis process may contribute something to the enhanced photocatalytic activity. Furthermore, the spherical morphology of the TiO_2 catalyst can also increase the light scattering during the photocatalytic reaction, and thus can effectively make better use of the UV light, further enhancing the photocatalytic activity.[57] Generally, after the Pt loading, a 60- to 120-fold increase of H_2 can be generated compared with the plain TiO_2 sphere catalyst, indicating that the H_2 generation reaction through photodriven water splitting is considerably accelerated by Pt. As mentioned previously, H_2 can accelerate the reduction of CO_2 to CH_4, and as a result, after the Pt loading, TiO_2 sphere catalysts also produce higher CH_4 than the plain catalyst. In particular, the Pt (0.6 wt %)/TiO_2 sphere catalyst exhibits the highest production of CH_4, i.e., ca. 20 times higher CH_4 production than Degussa P25 TiO_2. This value is also more than 2 times higher than that observed for Pt (0.6 wt %)/P25 TiO_2.

Although the TiO_2 sphere-based catalyst developed here has demonstrated greatly enhanced photocatalytic activity toward photodriven CO_2 reduction with water, there is still much potential for further improvement of these catalysts. First, one can synthesize TiO_2 spheres with smaller dimensions (e.g., 0.8 and 0.5 mm, Supporting Information) to increase surface area, and with other morphologies, such as hollow TiO_2 spheres, in which the hollow core can be expected to facilitate fast mass transport.[58−63] Jiao et al. reported that compared with a solid TiO_2 crystal, hollow TiO_2 crystals and mesocrystals can substantially improve photocatalytic activity (O_2/H_2 evolution from water splitting, CH_4 generation from photoreduction of CO_2) as a result of the synergistic effects of a shortened bulk diffusion length for the carriers resulting in decreased bulk recombination, and increased surface area.[64] Second, it has been reported that Pt particle size plays an important role in the CO_2 photoreduction process,[65] and hence, a better synthesis strategy is expected to reduce the particle size of deposited Pt particles, which will enhance the utilization efficiency of the Pt NPs. At present, Pt (0.6 wt %)/TiO_2 has Pt NPs of ca. 12 nm in size. Large Pt NPs may consume holes, thus serving as recombination centers.[65] If a better synthesis method is applied, the Pt nanoparticle size is expected to decrease significantly.[66] With smaller particle size and a more uniform dispersion of Pt NPs on the TiO_2 substrate, the photocatalytic activity of the Pt-loaded TiO_2-based catalysts is expected to improve greatly. Third, some metal elements such as Cu (Fe, Sn) or their oxides can be utilized as co-promoters to further enhance photocatalytic activity of the Pt-loaded TiO_2 sphere-based catalyst.

Presently, we have designed and built a photocatalytic UV-irradiated (or solar light) fluidized bed reactor with an approximate 0.5 L reactor volume, as shown in Figure S6. The fluidized bed reactor should improve efficiency and scalability of the photocatalytic process using the new TiO_2 sphere-based catalysts. Uner et al. reported that a fluidized bed reactor performs better than a fixed bed reactor for CO_2 photoconversion and hydrocarbon selectivity because the former has high active surface area and beneficial mass-transport conditions.[67] However, some post-processes were required after use such as filtration, centrifugation, and flocculation to recover powder-type photocatalysts in the slurry. Furthermore, there are some other problems such as the agglomeration, condensation of NPs, and reduced light penetration in the slurry. To solve this problem, we have developed catalysts with a larger particle size (i.e., the as-prepared Pt-loaded TiO_2 spheres of ca. 1.3 mm in diameter). The fluidized bed reactor has been used successfully for photocatalytic water splitting,[18] and the plan is to use it for the photocatalytic conversion of CO_2 to fuels.

4. CONCLUSIONS

Spherical TiO_2 based photocatalysts with large particle size (ca. 1.3 mm) have been developed and explored for photodriven CO_2 reduction with water to chemical fuels in single-compartment batch reactors. It was found that the spherical TiO_2-based catalyst demonstrates much better selectivity to reduce CO_2 to the end product, CH_4. On the basis of the yield of CH_4, the spherical TiO_2 catalyst exhibits 4 to 5 times the conversion rate of CO_2 reduction that can be obtained by the commercial Degussa P25 TiO_2 catalyst. This is mainly attributable to the superior surface and structural characteristics of the former, i.e., larger surface area and mesoporous volume, and particularly the hierarchical porosity, which is beneficial to fast mass transport and enhanced light harvesting. After Pt loading, the yield of CH_4 is further enhanced. With a Pt loading of 0.6 wt %, the spherical TiO_2-based catalyst exhibits a CH_4 production rate ca. 20 times greater than that produced by Degussa P25 TiO_2, indicating that the spherical TiO_2-based catalysts are very promising for photodriven CO_2 reduction. There is also significant potential for further improvement of the photocatalytic performance for spherical TiO_2-based catalysts. Approaches would include using hollow TiO_2 spheres, depositing Pt NPs with smaller particle size, and incorporating Cu (Fe, Sn) as a co-promoter. Some of the work involving these approaches is already in progress. In addition to the study with the batch reactors, we have also developed a fluidized bed reactor, which can be used for scalable CO_2 reduction and H_2O splitting processes. The spherical based photocatalysts with particle size greater than several hundreds of micrometers are ideally suited to these scalable processes.

■ ASSOCIATED CONTENT

Ⓢ Supporting Information

Photographs for the experimental setup, SEM images for TiO_2 spheres with various particle size, SEM images for commercial Degussa P25 TiO_2, SEM images for the Pt (1.8 wt %)/TiO_2 spheres, the XRD pattern for Pt black, and a photograph for a photocatalytic UV-irradiated fluidized bed reactor. This material is available free of charge via the Internet at http://pubs.acs.org.

■ AUTHOR INFORMATION

Corresponding Author

*Phone: +1-604-8224888. E-mail: dwilkinson@chbe.ubc.ca.

Notes

The authors declare no competing financial interest.

■ ACKNOWLEDGMENTS

The authors would like to thank Carbon Management Canada (CMC project B222) and the Pacific Institute for Climate Solutions (PICS) for financial support, and to thank Dr. Alfred Lam and Greg Afonso for help with designing and fabricating the reactors.

■ REFERENCES

(1) Pomoni, K.; Vomvas, A.; Trapalis, C. Transient Photoconductivity of Nanocrystalline TiO_2 Sol-Gel Thin Films. *Thin Solid Films* **2005**, *479*, 160−165.

(2) Ksibi, M.; Rossignol, S.; Tatibouet, J.; Trapalis, C. Synthesis and Solid Characterization of Nitrogen and Sulfur-Doped TiO_2 Photocatalysts Active under Near Visible Light. *Mater. Lett.* **2008**, *62*, 4204−4206.

(3) Devi, L.; Kottam, N.; Kumar, S. Preparation and Characterization of Mn-Doped Titanates with a Bicrystalline Framework: Correlation of the Crystallite Size with the Synergistic Effect on the Photocatalytic Activity. *J. Phys. Chem. C* **2009**, *113*, 15593−15601.

(4) Liu, S.; Yu, J.; Jaroniec, M. Tunable Photocatalytic Selectivity of Hollow TiO_2 Microspheres Composed of Anatase Polyhedra with Exposed {001} Facets. *J. Am. Chem. Soc.* **2010**, *132*, 11914−11916.

(5) Wen, C.; Jiang, H.; Qiao, S.; Yang, H.; Lu, G. Synthesis of High-Reactive Facets Dominated Anatase TiO_2. *J. Mater. Chem.* **2011**, *21*, 7052−7061.

(6) Li, Q.; Guo, B.; Yu, J.; Ran, J.; Zhang, B.; Yan, H.; Gong, J. Highly Efficient Visible-Light-Driven Photocatalytic Hydrogen Production of CdS-Cluster-Decorated Graphene Nanosheets. *J. Am. Chem. Soc.* **2011**, *133*, 10878−10884.

(7) Xiang, Q.; Yu, J.; Jaroniec, M. Graphene-Based Semiconductor Photocatalysts. *Chem. Soc. Rev.* **2012**, *41*, 782−796.

(8) Wang, W.; Yu, J.; Xiang, Q.; Cheng, B. Enhanced Photocatalytic Activity of Hierarchical Macro/Mesoporous TiO_2−Graphene Composites for Photodegradation of Acetone in Air. *Appl. Catal., B* **2012**, *119*, 109−116.

(9) Wang, H.; Sun, F.; Zhang, Y.; Li, L.; Chen, H.; Wu, Q.; Yu, J. Photochemical Growth of Nanoporous SnO_2 at the Air−Water Interface and Its High Photocatalytic Activity. *J. Mater. Chem.* **2010**, *20*, 5641−5645.

(10) Fan, S.; Kim, D.; Kim, J.; Jung, D.; Kang, S.; Ko, J. Highly Efficient CdSe Quantum-Dot-Sensitized TiO_2 Photoelectrodes for Solar Cell Applications. *Electrochem. Commun.* **2009**, *11*, 1337−1339.

(11) Fan, S.; Geng, Y.; Kim, C.; Park, S.; Ko, J. Correlating the Photovoltaic Performance of Alumina Modified Dye-Sensitized Solar Cells with the Properties of Metal-Free Organic Sensitizers. *Mater. Chem. Phys.* **2012**, *132*, 943−949.

(12) Pan, X.; Yang, M.; Fu, X.; Zhang, N.; Xu, Y. Defective TiO_2 with Oxygen Vacancies: Synthesis, Properties and Photocatalytic Applications. *Nanoscale* **2013**, *5*, 3601−3614.

(13) Inoue, T.; Fujishima, A.; Konishi, S.; Honda, K. Photoelectrocatalytic Reduction of Carbon Dioxide in Aqueous Suspensions of Semiconductor Powders. *Nature* **1979**, *277*, 637−638.

(14) Barton, E.; Rampulla, D.; Bocarsly, A. Selective Solar-Driven Reduction of CO_2 to Methanol Using a Catalyzed p-GaP Based Photoelectrochemical Cell. *J. Am. Chem. Soc.* **2008**, *130*, 6342−6344.

(15) Ishida, H.; Terada, T.; Tanaka, K.; Tanaka, T. Electrochemical CO_2 Reduction Catalyzed by Ruthenium Complexes $[Ru(bpy)_2(CO)_2]^{2+}$ and $[Ru(bpy)_2(CO)Cl]^+$. Effect of pH on the Formation of CO and $HCOO^-$. *Organometallics* **1987**, *6*, 181−186.

(16) Hawecker, J.; Lehn, J.; Ziessel, R. Efficient Photochemical Reduction of CO_2 to CO by Visible Light Irradiation of Systems Containing $Re(bipy)(CO)_3X$ or $Ru(bipy)_3^{2+}$−Co^{2+} Combinations as Homogeneous Catalysts. *J. Chem. Soc., Chem. Commun.* **1983**, 536−538.

(17) Takeda, H.; Koike, K.; Inoue, H.; Ishitani, O. Development of An Efficient Photocatalytic System for CO_2 Reduction Using Rhenium(I) Complexes Based on Mechanistic Studies. *J. Am. Chem. Soc.* **2008**, *130*, 2023−2031.

(18) Reilly, K.; Taghipour, F.; Wilkinson, D. Photocatalytic Hydrogen Production in a UV-Irradiated Fluidized Bed Reactor. *Energy Procedia* **2012**, *29*, 513−521.

(19) Khan, M.; Akhtar, M.; Woob, S.; Yang, O. Enhanced Photoresponse under Visible Light in Pt Ionized TiO_2 Nanotube for the Photocatalytic Splitting of Water. *Catal. Commun.* **2008**, *10*, 1−5.

(20) Indrakanti, V.; Kubicki, J.; Schobert, H. Photoinduced Activation of CO_2 on Ti-Based Heterogeneous Catalysts: Current State, Chemical Physics-Based Insights and Outlook. *Energy Environ. Sci.* **2009**, *2*, 745−758.

(21) Lv, K.; Xiang, Q.; Yu, J. Effect of Calcination Temperature on Morphology and Photocatalytic Activity of Anatase TiO_2 Nanosheets with Exposed {001} Facets. *Appl. Catal., B* **2011**, *104*, 275−281.

(22) Yu, J.; Su, Y.; Cheng, B. Template-Free Fabrication and Enhanced Photocatalytic Activity of Hierarchical Macro-/Mesoporous Titania. *Adv. Funct. Mater.* **2007**, *17*, 1984−1990.

(23) Lo, C.; Hung, C.; Yuan, C.; Wu, J. Photoreduction of Carbon Dioxide with H_2 and H_2O over TiO_2 and ZrO_2 in a Circulated Photocatalytic Reactor. *Sol. Energy Mater. Sol. Cells* **2007**, *91*, 1765−1774.
(24) Tan, S.; Zou, L.; Hu, E. Photosynthesis of Hydrogen and Methane as Key Components for Clean Energy System. *Sci. Technol. Adv. Mater.* **2007**, *8*, 89−92.
(25) Tan, S.; Zou, L.; Hu, E. Photocatalytic Production of Methane and Hydrogen Through Reduction of Carbon Dioxide with Water Using Titania Pellets. *Int. J. Green Energy* **2006**, *3*, 283−290.
(26) Varghese, O.; Paulose, M.; LaTempa, T.; Grimes, C. A. High-Rate Solar Photocatalytic Conversion of CO_2 and Water Vapor to Hydrocarbon Fuels. *Nano Lett.* **2009**, *9*, 731−737.
(27) Roy, S.; Varghese, O.; Paulose, M.; Grimes, C. Toward Solar Fuels: Photocatalytic Conversion of Carbon Dioxide to Hydrocarbons. *ACS Nano* **2010**, *4*, 1259−1278.
(28) Ma, Q.; Liu, S.; Weng, L.; Liu, Y.; Liu, B. Growth, Structure and Photocatalytic Properties of Hierarchical Cu−Ti−O Nanotube Arrays by Anodization. *J. Alloys Compd.* **2010**, *501*, 333−338.
(29) Mor, G.; Prakasam, H.; Varghese, O.; Shankar, K.; Grimes, C. Vertically Oriented Ti−Fe−O Nanotube Array Films: Toward a Useful Material Architecture for Solar Spectrum Water Photoelectrolysis. *Nano Lett.* **2007**, *7*, 2356−2364.
(30) Tu, Y.; Huang, S.; Sang, J.; Zou, X. Synthesis and Photocatalytic Properties of Sn-Doped TiO_2 Nanotube Arrays. *J. Alloys Compd.* **2009**, *482*, 382−387.
(31) Xia, X.; Jia, Z.; Yu, Y.; Liang, Y.; Wang, Z.; Ma, L. Preparation of Multi-Walled Carbon Nanotube Supported TiO_2 and Its Photocatalytic Activity in the Reduction of CO_2 with H_2O. *Carbon* **2007**, *45*, 717−721.
(32) Sasirekha, N.; Basha, S.; Shanthi, K. Photocatalytic Performance of Ru Doped Anatase Mounted on Silica for Reduction of Carbon Dioxide. *Appl. Catal., B* **2006**, *62*, 169−178.
(33) Dubois, M.; Dubios, D. Development of Molecular Electrocatalysts for CO_2 Reduction and H_2 Production/Oxidation. *Acc. Chem. Res.* **2009**, *42*, 1974−1982.
(34) Tan, L.; Kumar, M.; An, W.; Gao, H. Transparent, Well-Aligned TiO_2 Nanotube Arrays with Controllable Dimensions on Glass Substrates for Photocatalytic Applications. *ACS Appl. Mater. Interfaces* **2010**, *2*, 498−503.
(35) Indrakanti, V.; Schobert, H.; Kubicki, J. Quantum Mechanical Modeling of CO_2 Interactions with Irradiated Stoichiometric and Oxygen-Deficient Anatase TiO_2 Surfaces: Implications for the Photocatalytic Reduction of CO_2. *Energy Fuels* **2009**, *23*, 5247−5256.
(36) Wang, C.; Thompson, R. L.; Baltrus, J.; Matranga, C. Visible Light Photoreduction of CO_2 Using CdSe/Pt/TiO_2 Heterostructured Catalysts. *J. Phys. Chem. Lett.* **2010**, *1*, 48−53.
(37) Liu, G.; Hoivik, N.; Wang, K.; Jakobsen, H. Engineering TiO_2 Nanomaterials for CO_2 Conversion/Solar Fuels. *Sol. Energy Mater. Sol. Cells* **2012**, *105*, 53−68.
(38) Mori, K.; Yamashita, H.; Anpo, M. Photocatalytic Reduction of CO_2 with H_2O on Various Titanium Oxide Photocatalysts. *RSC Adv.* **2012**, *2*, 3165−3172.
(39) Adrian A. V. Development and Evaluation of a Composite Photocatalyst for Water Treatment Processes. Ph.D. Thesis, University of British Columbia, British Columbia, Canada, 2009.
(40) Fang, B.; Kim, J.; Kim, M.; Yu, J. Ordered Hierarchical Nanostructured Carbon as a Highly Efficient Cathode Catalyst Support in Proton Exchange Membrane Fuel Cell. *Chem. Mater.* **2009**, *21*, 789−796.
(41) Fang, B.; Chaudhari, N.; Kim, M.; Kim, J.; Yu, J. Homogeneous Deposition of Platinum Nanoparticles on Carbon Black for Proton Exchange Membrane Fuel Cell Application. *J. Am. Chem. Soc.* **2009**, *131*, 15330−15338.
(42) Fang, B.; Kim, M.; Kim, J.; Song, M.; Wang, Y.; Wang, H.; Wilkinson, D.; Yu, J. High Pt Loading on Functionalized Multiwall Carbon Nanotube as a Highly Efficient Cathode Electrocatalyst for Proton Exchange Membrane Fuel Cell. *J. Mater. Chem.* **2011**, *21*, 8066−8073.
(43) Liu, G.; Hoivik, N.; Wang, K.; Jakosen, H. Engineering TiO_2 Nanomaterials for CO_2 Conversion/Solar Fuels. *Sol. Energy Mater. Sol. Cells* **2012**, *105*, 53−68.
(44) Centi, G.; Perathoner, S. Towards Solar Fuels from Water and CO_2. *ChemSusChem* **2010**, *3*, 195−208.
(45) Yu, J.; Qi, L.; Jaroniec, M. Hydrogen Production by Photocatalytic Water Splitting over Pt/TiO_2 Nanosheets with Exposed (001) Facets. *J. Phys. Chem. C* **2010**, *114*, 13118−13125.
(46) Loganathan, K.; Bommusamy, P.; Muthaiahpillai, P.; Velayutham, M. The Syntheses, Characterizations, and Photocatalytic Activities of Silver, Platinum, and Gold Doped TiO_2 Nanoparticles. *Environ. Eng. Res.* **2011**, *16*, 81−90.
(47) Shah, S.; Li, W.; Huang, C.; Jung, O.; Ni, C. Study of Nd^{3+}, Pd^{2+}, Pt^{4+}, and Fe^{3+} Dopant Effect on Photoreactivity of TiO_2 Nanoparticles. *Proc. Natl. Acad. Sci. U.S.A.* **2002**, *99*, 6482−6486.
(48) Li, Y.; Wang, W.; Zhan, Z.; Woo, M.; Wu, C.; Biswas, P. Photocatalytic Reduction of CO_2 with H_2O on Mesoporous Silica Supported Cu/TiO_2 Catalysts. *Appl. Catal., B* **2010**, *100*, 386−392.
(49) Izumi, Y. Recent Advances in the Photocatalytic Conversion of Carbon Dioxide to Fuels with Water and/or Hydrogen Using Solar Energy and Beyond. *Coord. Chem. Rev.* **2003**, *257*, 171−186.
(50) Zhao, T.; Liu, Z.; Nakata, K.; Nishimoto, S.; Murakami, T.; Zhao, Y.; Jiang, L.; Fujishima, A. Multichannel TiO_2 Hollow Fibers with Enhanced Photocatalytic Activity. *J. Mater. Chem.* **2010**, *20*, 5095−5099.
(51) Yin, C.; Zhu, S.; Chen, Z.; Zhang, W.; Gu, J.; Zhang, D. One Step Fabrication of C-Doped $BiVO_4$ with Hierarchical Structures for a High-Performance Photocatalyst under Visible Light Irradiation. *J. Mater. Chem. A* **2013**, *1*, 8367−8378.
(52) Zhu, S.; Zhang, D.; Chen, Z.; Zhou, G.; Jiang, H.; Li, J. Sonochemical Fabrication of Morpho-Genetic TiO_2 with Hierarchical Structures for Photocatalyst. *J. Nanopart. Res.* **2010**, *12*, 2445−2456.
(53) Li, H.; Bian, Z.; Zhu, J.; Zhang, D.; Li, G.; Huo, Y.; Li, H.; Lu, Y. Mesoporous Titania Spheres with Tunable Chamber Structure and Enhanced Photocatalytic Activity. *J. Am. Chem. Soc.* **2007**, *129*, 8406−8407.
(54) Kiwi, J.; Gratzel, M. Optimization of Conditions for Photochemical Water Cleavage. Aqueous Platinum/TiO_2 (Anatase) Dispersions under Ultraviolet Light. *J. Phys. Chem.* **1984**, *88*, 1302−1307.
(55) Wang, X.; Yu, J.; Ho, C.; Hou, Y.; Fu, X. Photocatalytic Activity of a Hierarchically Macro/Mesoporous Titania. *Langmuir* **2005**, *21*, 2552−2559.
(56) Liu, S.; Yu, J. Cooperative Self-Construction and Enhanced Optical Absorption of Nanoplates-Assembled Hierarchical Bi_2WO_6 Flowers. *J. Solid State Chem.* **2008**, *181*, 1048−1055.
(57) Liu, B.; Nakata, K.; Sakai, M.; Saito, H.; Ochiai, T.; Murakami, T.; Takagib, K.; Fujishima, A. Hierarchical TiO_2 Spherical Nanostructures with Tunable Pore Size, Pore Volume, and Specific Surface Area: Facile Preparation and High-Photocatalytic Performance. *Catal. Sci. Technol.* **2012**, *2*, 1933−1939.
(58) Fang, B.; Kim, J.; Kim, M.; Bonakdarpour, A.; Lam, A.; Wilkinson, D.; Yu, J. Fabrication of Hollow Core Carbon Spheres with Hierarchical Nanoarchitecture for Ultrahigh Electrical Charge Storage. *J. Mater. Chem.* **2012**, *22*, 19031−19038.
(59) Kim, J.; Fang, B.; Song, M.; Yu, J. Topological Transformation of Thioether-Bridged Organosilicas into Nanostructured Functional Materials. *Chem. Mater.* **2012**, *24*, 2256−2264.
(60) Kim, M.; Fang, B.; Kim, J.; Yang, D.; Kim, Y.; Bae, T.; Yu, J. Ultra- High Li Storage Capacity Achieved by Hollow Carbon Capsule with Hierarchical Nanoarchitecture. *J. Mater. Chem.* **2011**, *21*, 19362−19367.
(61) Fang, B.; Kim, M.; Yu, J. Hollow Macroporous Core/Mesoporous Shell Carbon as Highly Efficient Catalyst Support in Direct Formic Acid Fuel Cell. *Appl. Catal., B* **2008**, *84*, 100−105.
(62) Fang, B.; Kim, J.; Kim, M.; Yu, J. Controllable Synthesis of Hierarchical Nanostructured Hollow Core/Mesopore Shell Carbon for Electrochemical Hydrogen Storage. *Langmuir* **2008**, *24*, 12068−12072.

(63) Fang, B.; Kim, J.; Kim, M.; Yu, J. Hierarchical Nanostructured Carbons with Meso-Macroporosity: Design, Characterization and Applications. *Acc. Chem. Res.* **2013**, *46*, 1397−1406.
(64) Jiao, W.; Wang, L.; Liu, G.; Lu, G.; Cheng, H. Hollow Anatase TiO_2 Single Crystals and Mesocrystals with Dominant {101} Facets for Improved Photocatalysis Activity and Tuned Reaction Preference. *ACS Catal.* **2012**, *2*, 1854−1859.
(65) Wang, W.; An, W.; Ramalingam, B.; Mukherjee, S.; Niedzwiedzki, D.; Gangopadhyay, S.; Biswas, P. Size and Structure Matter: Enhanced CO_2 Photoreduction Efficiency by Size-Resolved Ultrafine Pt Nanoparticles on TiO_2 Single Crystals. *J. Am. Chem. Soc.* **2012**, *134*, 11276−11281.
(66) Xie, Y.; Ding, K.; Liu, Z.; Tao, R.; Sun, Z.; Zhang, H.; An, G. In Situ Controllable Loading of Ultrafine Noble Metal Particles on Titania. *J. Am. Chem. Soc.* **2009**, *131*, 6648−6649.
(67) Uner, D.; Oymak, M. On the Mechanism of Photocatalytic CO_2 Reduction with Water in the Gas Phase. *Catal. Today* **2012**, *181*, 82−88.